galaxies

MDPI

Article

# ALMA's Acute View of pPNe: Through the Magnifying Glass... and What We Found There

**Carmen Sánchez Contreras [1,*], Javier Alcolea [2], Valentín Bujarrabal [3] and Arancha Castro-Carrizo [4]**

1 Centro de Astrobiología (CSIC-INTA), Camino Bajo del Castillo s/n, Urb. Villafranca del Castillo, 28691 Villanueva de la Cañada, Spain
2 Observatorio Astronómico de Madrid, Observatorio Astronómico Nacional (IGN), Alfonso XII No 3, 28014 Madrid, Spain; j.alcolea@oan.es
3 Centro de Investigaciones de Ciencias Geográficas y Astronomía, Observatorio Astronómico Nacional (IGN), Ap 112, 28803 Alcalá de Henares, Spain; vbujarrabal@oan.es
4 Institut de Radioastronomie Millimetrique, 300 rue de la Piscine, 38406 Saint Martin d'Heres, France; ccarrizo@iram.fr
* Correspondence: csanchez@cab.inta-csic.es; Tel.: +34-918-131-205

Received: 28 June 2018; Accepted: 20 August 2018; Published: 4 September 2018


**Abstract:** We present recent Atacama Large Millimeter/submillimeter Array (ALMA)-based studies of circumstellar envelopes (CSEs) around Asymptotic Giant Branch (AGB) stars and pre-Planetary Nebulae (pPNe). In only a few years of operation, ALMA is revolutionising the field of AGB-to-PN research by providing unprecedentedly detailed information on the complex nebular architecture (at large but also on small scales down to a few ∼10 AU from the centre), dynamics and chemistry of the outflows/envelopes of low-to-intermediate mass stars in their late stages of the evolution. Here, we focus on continuum and molecular line mapping studies with high angular resolution and sensitivity of some objects that are key to understanding the complex PN-shaping process. In particular, we offer (i) a brief summary of ALMA observations of rotating disks in post-AGB objects and (ii) report on ALMA observations of OH 231.8+4.2 providing the most detailed and accurate description of the global nebular structure and kinematics of this iconic object to date.

**Keywords:** AGB and post-AGB stars; circumstellar matter; winds and outflows; mass-loss; jets

## 1. Introduction

Due to its unique capabilities, the Atacama Large Millimeter/submillimeter Array (ALMA) has an immense potential to make great advances, and to answer major questions, in the field of Asymptotic Giant Branch (AGB)-to-Planetary Nebulae (PNe) evolution. The first ALMA images of an AGB star, R Sculptoris [1], showed a spiral structure inscribed in the circumstellar envelope (CSE), and, for the first time, astronomers could get full three-dimensional information about this outrageous structure, created by a hidden companion star orbiting the red giant. These ALMA maps were the prelude for future discoveries and marked the beginning of a new era in AGB/post-AGB/pre-Planetary Nebulae (pPNe)/PNe research.

At the time of giving this presentation, i.e., during the Asymmetric Planetary Nebulae (APN) VII meeting, ALMA was in cycle five, offering already excellent angular resolution over a broad range of frequencies (from ∼100 to ∼870 GHz). At 1 mm the angular resolution was below 20 milliarcsec, which represents an improvement of more than a factor of 10 with respect to other mm/sub-mm-interferometers. This resolution enables us (i) to obtain a close up view of the central regions of pPNe and to look for relevant structures that are directly related to, or take part in, the wind

collimation process and (ii) to gather a very detailed characterization of large-scale structures (and to discover new ones) that can help us to build up the nebular shaping history of these objects. In this presentation, we show some examples of these two types of studies. In Section 2, a very brief summary of ALMA observations of rotating disks in post-AGB objects is offered. In Section 3, we present (a small part of) our ALMA observations of OH 231.8+4.2, a key object to understand PN-shaping.

## 2. A Quest for Rotating Disks in Post-AGB Objects

Rotating disks are invoked by most wind collimation theories, e.g., [2–4], and are suspected to be present in a particular class of post-AGB stars with near-IR emission excess (see [5] for a review). The near-IR emission excess indicates hot dust located in a stable disk-like structure close to the star (at $\approx 10^{14}$–$10^{15}$ cm). In contrast to most pPNe, these objects show narrow CO emission profiles consistent with rotating disks [6]. The prototype of this class of post-AGB objects is the Red Rectangle, which was the first source in which a Keplerian disk was directly confirmed and spatially resolved with interferometric CO emission observations [7]. Modelling of these data enabled a detailed characterization of the structure and kinematics of the disk, as well as an estimate of the mass of the central binary system of $\sim 1.5\, M_{\odot}$.

More recently, several molecular transitions in the Red Rectangle have been mapped with ALMA with better angular resolution and sensitivity [8,9]. This has enabled not only an improved characterization of the disk, but has also revealed the presence of a tenuous X-shaped wind that emanates from the disk at the low velocity of $\sim$3–10 km s$^{-1}$. The mass–loss rate of the wind, which may be material photoevaporating from the disk, implies a lifetime of the disk of $\sim$5000–10,000 yr.

The quest for rotating disks continues, and more post-AGB objects with near-IR excess are being observed in CO emissions. IW Car [10] and IRAS 08544-4133 [11] are the most recent examples of post-AGB stars in which rotating disks and winds emerging from the disk have been spatially resolved with ALMA. Rotating disks around post-AGB stars had been mapped earlier, also with the IRAM interferometer, e.g., 89 Her [12] and AC Her [13].

The properties of the disks and the X-winds (when detected) are similar in all post-AGB targets (Table 1), although a very low-number statistics still prevails. We emphasize that, given the large dimensions of the disks mapped to date (with typical outer radii of the order of 1000 AU), these structures do not represent the compact accretion disks (around the compact companion of the mass-lossing star) postulated by most wind-collimation theories. The rotating disks reported as of today are relatively large structures around the central binary system, typically with a total mass of $M_{\star} \sim$ 1–2 $M_{\odot}$. The role of these circumbinary disks in the wind collimation and/or, more generally, in the PN-shaping process, remains unclear. Recently, the first rotating disk in an AGB star, $L_2$ Pup, has been detected and spatially resolved with ALMA [14,15]. In this case, the disk is smaller and less massive than the post-AGB stars shown before, but it is also tentatively circumbinary.

Rotating disks in post-AGB objects have typical masses of $M_{disk} \approx 10^{-3}$–$10^{-2}\, M_{\odot}$, the Red Rectangle being the most massive detected so far, and excitation temperatures of $\approx$100 K. For objects where a rotating disk and an X-wind component are simultaneously detected, the mass of the latter is only a small fraction (10%) of the mass of the disk. These X-winds are very different from the massive ($\sim$0.1–1 $M_{\odot}$) and high-momentum bipolar outflows common to most pPNe [16]. It is paradoxical that none of the pPNe with massive, high-momentum bipolar outflows have shown clear evidence for rotation at their cores. Therefore, ironically, rotating disk are only found in objects where a powerful jet-launching engine does not need to be invoked. This is a mystery that ALMA will hopefully solve in the coming years, as more rotating disks and pPNe are observed.

**Table 1.** Keplerian circumbinary disks with CO interferometric maps.

| Name | Class | Disk | X-Wind | $R_{disk}$ | $M_{disk}$ | $M_\star$ | Reference |
|---|---|---|---|---|---|---|---|
| Red Rectangle | post-AGB | Yes | Yes | ≈2000 AU | $4.0 \times 10^{-2}\,M_\odot$ | $\sim 1.5\,M_\odot$ | [7–9] |
| IW Car | post-AGB | Yes | Yes | ≈1300 AU | $4.0 \times 10^{-3}\,M_\odot$ | $\sim 1\,M_\odot$ | [10] |
| AC Her | post-AGB | Yes | ? | ≈1130 AU | $1.5 \times 10^{-3}\,M_\odot$ | $\sim 1.5\,M_\odot$ | [13] |
| IRAS 08544 | post-AGB | Yes | Yes | ≈1400 AU | $6.0 \times 10^{-3}\,M_\odot$ | $\sim 1.8\,M_\odot$ | [11] |
| 89 Her | post-AGB | Possibly | Yes | $\lesssim$200 AU | $(\sim 10^{-2}\,M_\odot)$ | $(\sim 1\,M_\odot)$ | [12] |
| $L_2$ Pup | AGB | Yes | ? | ≈20 AU | $2.2 \times 10^{-4}\,M_\odot$ | $\sim 0.66\,M_\odot$ | [14,15] |

## 3. Nebular Architecture and Dynamics of pPNe: The ALMA View of OH 231.8+4.2

Characterization with ALMA of the nebular structure and dynamics of 'standard' pNe, i.e., with dominant bipolar outflows carrying a significant amount of mass and linear momentum, is essential to understand how they were formed. We show ALMA observations of OH 231.8+4.2, an object in a brief but key evolutionary stage of the AGB-to-PN transition.

OH 231.8+4.2 is an outstanding pPN-like nebula (Figure 1) around a Mira-type pulsating star (QX Pup). This uncommon situation makes OH 231.8+4.2 of special interest, since it demonstrates that asymmetries can develop (and become very prominent) while the central star is still on the AGB. OH 231.8+4.2 has been extensively studied at many wavelengths by several authors e.g., [17–24] (and references therein). The light from the central source inside OH 231.8's core is highly obscured by dust along the line-of-sight and is only seen indirectly scattered by the dust in the lobe walls, indicating the presence of an A 0-type main-sequence companion to the mass-losing AGB star, of spectral type M8-10 III [21]. It is believed that the bulk of the nebular mass, which is in the form of molecular gas ($\sim 1\,M_\odot$), has been ejected by the AGB star at a very high rate, $\dot{M} \approx 10^{-4}\,M_\odot\ \mathrm{yr}^{-1}$ [17]. Before ALMA came into play, two major large-scale components had been identified: (i) An equatorial waist expanding at low velocity, $<30\,\mathrm{km\,s^{-1}}$ and (ii) a highly collimated bipolar outflow with expansion velocities that increase linearly with the distance from the centre up to $\sim 400\,\mathrm{km\,s^{-1}}$ (deprojected). The linear velocity gradient in the outflow could have resulted from the sudden interaction between collimated fast winds (CFWs) on the ambient AGB material ∼800 yr ago.

We present a summary of our recent observations of OH 231.8+4.2 with ALMA. These data have provided us with a high-definition image of the dominant nebular components described above, but also, more importantly, have enabled us (1) to identify the position of the mass-losing star relative to the nebula and (2) to discover a number of outflow components previously unknown. We also report the first detection of $Na^{37}Cl$ and $CH_3OH$ in OH 231.8+4.2, with $CH_3OH$ also being a first detection around an AGB star. A comprehensive study of this dataset is reported by [25].

### 3.1. Observations

OH 231.8+4.2 was observed with the ALMA 12 m array as part of project 2015.1.00256.S on July 2016. We mapped the continuum emission and a series of spectral lines in band seven (∼294–345 GHz). Our project has two major science goals: SG1 is a five-point mosaic of $^{12}CO/^{13}CO$ (3-2) and other molecules covering a $\sim 19'' \times 54''$ area along the bipolar outflow, and SG2 is a single-pointing observation towards the centre to map a selection of lines, e.g., SiO and CS, amongst others. The resolution of these observations is ∼0.″2–0.″3. Full observational details are given in [25].

### 3.2. Continuum Maps

Maps of the continuum emission at four different frequencies (294, 304, 330 and 344 GHz) have been created using line-free channels. Our ∼294 GHz-continuum map is shown in the left panel of Figure 2 as an example. The surface brightness distribution, which is very similar at all frequencies, appears as an extended, incomplete hourglass-like structure, roughly oriented along PA $\sim 21^\circ$ (i.e., the symmetry axis of the large-scale nebula). The continuum emission distribution is

clumpy. The peak of the continuum maps is attained at one of these clumps, referred to as "*clump S*", which has coordinates R.A. = $07^{h}42^{m}16^{s}.915$ and Dec. = $-14°42'50''06$ (J2000). As we will show below, clump *S* enshrouds the central star QX Pup. We deduce a deconvolved radius of ∼40–70 AU for clump *S*, which is barely resolved. Note that clump *S* does not lie on the equatorial plane of the hourglass, but is clearly displaced along the axis towards the south by ∼0.″6. The total continuum flux with ALMA is consistent with that measured with single-dish telescopes (see right panel of Figure 2). Except for clump *S*, the spectral index of the continuum shows no significant deviations from a $S_\nu \propto \nu^{3.3}$ power-law across the different regions. This implies a dominant contribution by optically thin ∼75 K dust with an emissivity index of $\alpha$ ∼1.3. At clump *S*, the continuum obeys a $S_\nu \propto \nu^{2.1}$ dependence consistent with a population of large (>100 μm-sized) grains in the vicinity of QX Pup.

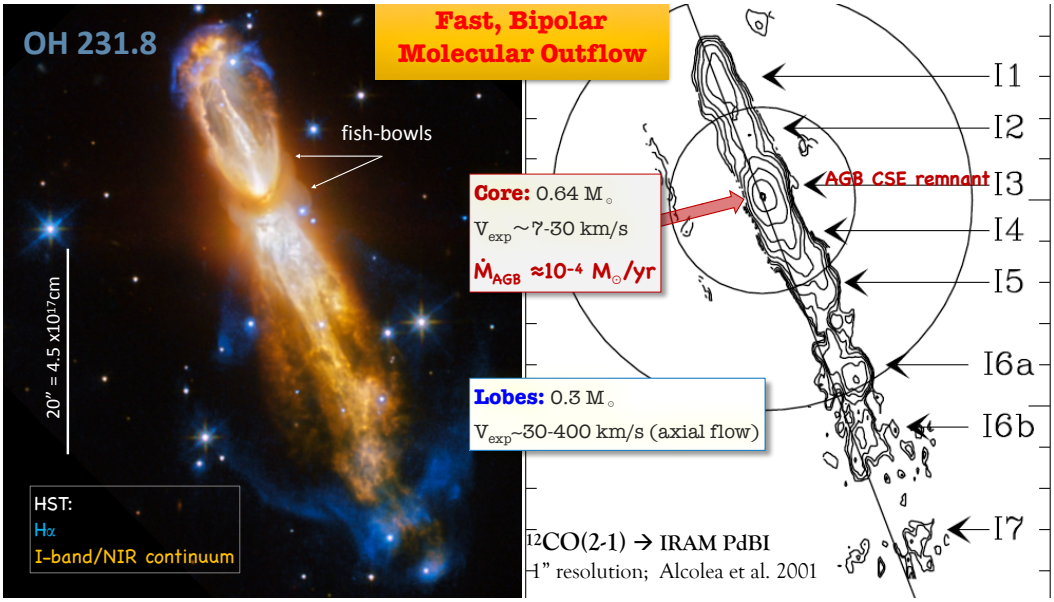


**Figure 1.** (**Left**) False color *HST* image of the reflection nebulosity (red-to-yellow) and H$\alpha$-emitting lobes (blue) of OH 231.8+4.2 (Credit: ESA/Hubble & NASA. Acknowledgement: Judy Schmidt). North is up. Two faint, bubble-like features (*fish-bowls*) with molecular counterparts in our ALMA data are indicated—see Section 3.3. (**Right**) ALMA order-zero moment maps of $^{12}$CO (2-1) integrated over the full width of the line profile adapted from [17]. The mass and expansion velocity of the low-velocity core and the fast, bipolar lobes are indicated. The distance to OH 231.8+4.2 is $d$∼1500 pc. The lobes are tilted with respect to the plane of the sky by $i$∼35°, with the North lobe being the closest.

### *3.3. Molecular Line Maps: Nebular Components*

We have mapped a large number of molecular transitions, covering a range of upper-level energies from $E_u$ ∼ 20 to 1800 K and including many species (CO, CS, SO, $SO_2$, SiO, SiS, $H_3O^+$, $CH_3OH$, etc.). Different lines are found to selectively (or exclusively) trace different components of the outflow, which facilitates disentangling the complex nebular architecture of OH 231.8+4.2. In the following, we describe different structures traced by ALMA, starting from the most compact ones (within $\approx 10^{15}$ cm from the mass-losing star) and ending with the most extended zones (reaching out to $\approx 10^{17}$ cm).

We have detected several high-excitation lines, namely, SiS ($v$ = 1, $J$ = 17 − 16), $^{30}$SiO ($v$ = 1, $J$ = 7 − 6), and Na$^{37}$Cl ($v$ = 0, $J$ = 26 − 25), with compact emission arising *entirely* from clump *S*. These lines are known to be produced in the warm inner ($\lesssim 10^{15}$ cm) layers of the winds of evolved mass-losing stars, where the stellar wind may have not reached its terminal expansion velocity. The emission is indeed confined to a small emitting volume of radius ∼60 AU (∼24$R_\star$), comparable to that of the

continuum-emitting core. The narrow profiles imply low expansion velocities of $V_{\rm exp} \sim 5$–$7\,{\rm km\,s^{-1}}$ in these layers, for which we deduce a kinematic age of about 50 yr.

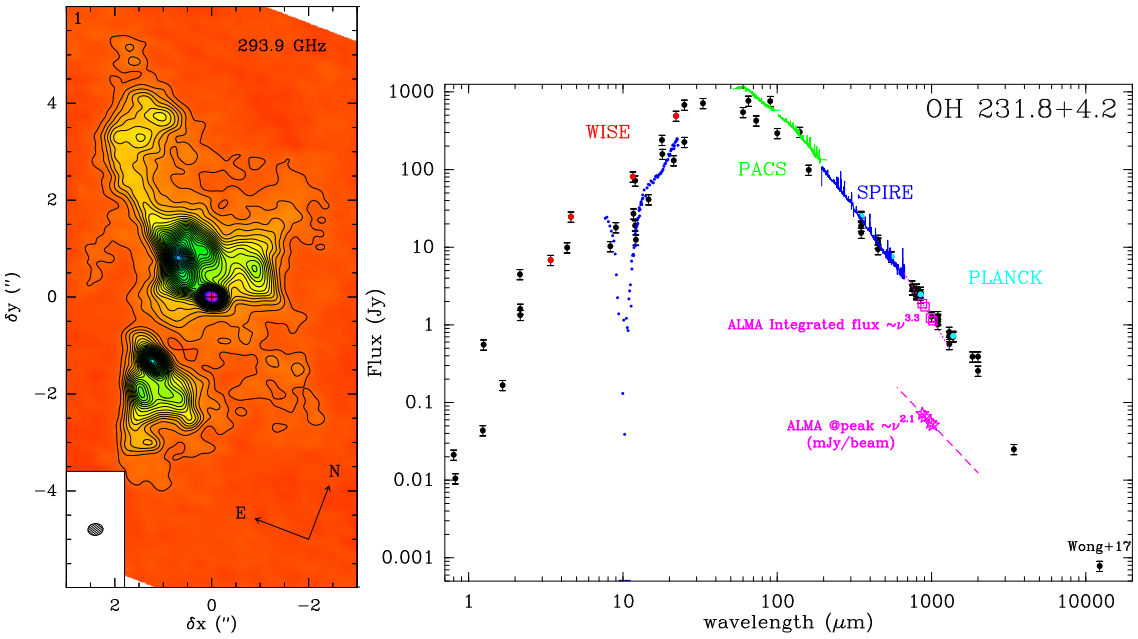


**Figure 2.** (**Left**) ALMA 294 GHz-continuum emission map of OH 231.8+4.2. Contour level spacing is 0.8 mJy/beam. The clean beam (HPBW = 0.″31 × 0.″25, PA = −84.5°) is plotted at the bottom-left corner. The compact region at the centre where the continuum emission peaks is referred to as clump *S* and it is a dust (and gas) region enshrouding the AGB star QX Pup. (**Right**) Spectral energy distribution. Pink symbols are our ALMA continuum measurements (squares = integrated flux; stars = peak-flux surface density at clump *S*) and the dotted and dashed lines are $S_\nu \propto \nu^{3.3}$ and $S_\nu \propto \nu^{2.1}$ fitted to those.

In addition to disclosing the locus of QX Pup inside clump *S*, we have discovered a compact ($\sim 1'' \times 4''$) bipolar outflow that emerges from the stellar vicinity. This outflow is exclusively sampled in our data by the SiO molecule, which is a well-known shock tracer (top panels of Figure 3). Our maps show a pair of flame-shaped lobes expanding at moderate velocities and oriented similarly to the large-scale nebula. The radial (or line-of-sight) velocity increases abruptly from the centre to two bright and compact regions located at offsets $\delta{\rm y} \sim \pm 0.''11$ about clump *S*, where the maximum radial velocities ($\sim 35\,{\rm km\,s^{-1}}$) and full line widths ($\sim 23\,{\rm km\,s^{-1}}$) are observed. These SiO-bright regions may represent bow-shocks, denoting recent ($\lesssim$50–80 yr old) bipolar mass ejections. The lower velocities at the intermediate-to-outer regions of the flame-shaped SiO-lobes imply larger kinematic ages of $t_{\rm kin} \sim 400$–$500$ yr.

Adjacent to the SiO-outflow, we identify a small-scale hourglass-shaped structure (*mini-hourglass*) that is probably made of compressed material formed as the SiO-outflow penetrates the dense, central regions of the nebula (bottom panels of Figure 3). The lobes and the equatorial waist of the mini-hourglass *both* are radially expanding with a constant velocity gradient ($V_{\rm exp} \propto r$). The dimensions and kinematics of the mini-waist are consistent with a torus-like structure with an outer radius of about 500 AU orthogonal to, and coeval with, the SiO-outflow. The expansion velocity at the inner edge of the mini-waist ($\sim$150 AU) is extremely low, at $V_{\rm exp} \sim 1\,{\rm km\,s^{-1}}$.

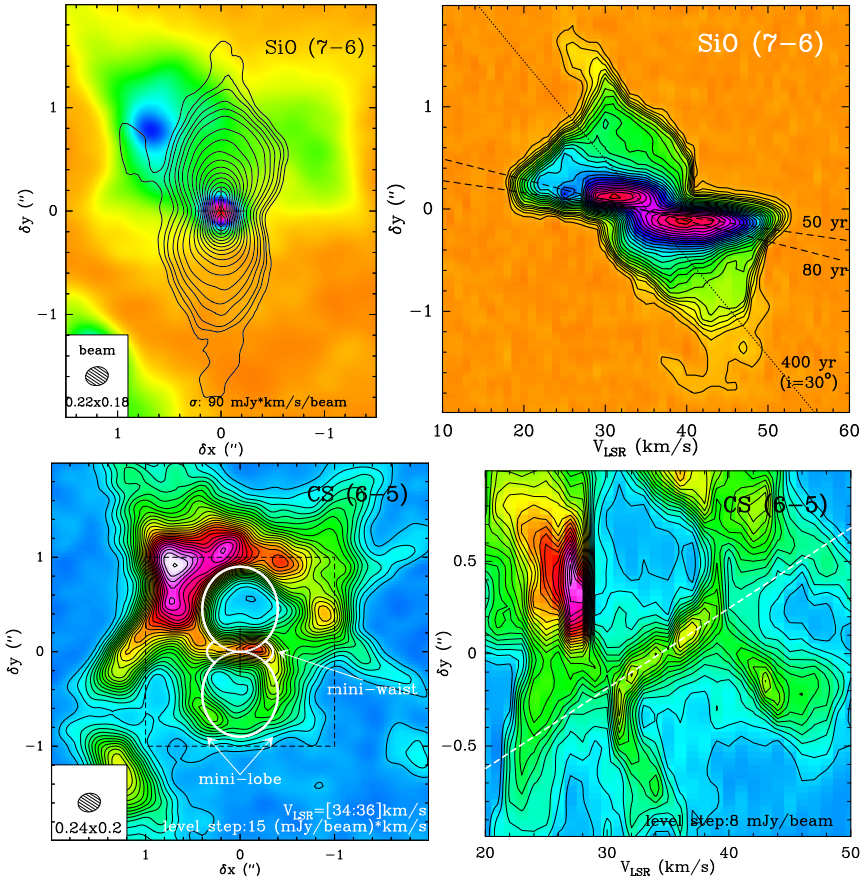


**Figure 3.** SiO (7−6) and CS (6−5) emission in OH 231.8+4.2. (**Left**) Zero-order moment maps (integrated over $V_{\rm LSR}$ = [18:53] and [34:36] km s$^{-1}$, for SiO and CS, respectively). The mini-hourglass centred at clump *S* is schematically depicted in the bottom-left panel. (**Right**) Position-velocity (PV) diagrams along PA = 21°. The lines represent different velocity gradients implying different kinematic ages at various regions of the SiO-outflow (top) and along the mini-waist (bottom).

The ∼8″ × 4″-sized hourglass nebula traced by the dust thermal continuum emission maps is the major emission component of most of the species mapped by us with ALMA. In Figure 4, we offer a condensed view of CS (7−6), one of the dense gas tracers observed by us, where this component is clearly seen. The large-hourglass is characterized by a dominant expansive kinematics described by a radial velocity gradient, $\nabla v \sim 6.0$–$6.5\,{\rm km\,s^{-1}\,arcsec^{-1}}$, that is sustained from the base to the tips of the lobes, where the highest velocities are observed. The sharp outer boundary of the large-waist is now accurately determined (at a radius of ∼2700 AU) as well as its internal velocity field, indicating that the waist was shaped nearly simultaneously with the high-velocity (HV) lobes, about 800–900 yr ago.

We report the discovery of two large (∼8″ × 6″) faint, bubble-like structures surrounding the central parts of the nebula (*fish-bowls*, see Figure 5). These are the molecular counterparts of the two faint, rounded structures seen in the *HST*/NIR images (Figure 1). The north and the south fish-bowls have similar dimensions, but are oriented differently. The observed spatio-kinematic distribution is consistent with the fish-bowls being a pair of hollow, thin-walled ellipsoids (probably made of swept up ambient material) radially expanding and moving away from each other. They are relatively old structures although apparently slightly (∼100–200 yr) younger than the large-scale waist and the HV-lobes. The origin of these enigmatic structures is unknown, but it may be linked to a 'critical' time period or instant of the evolution/development of the HV-lobes.

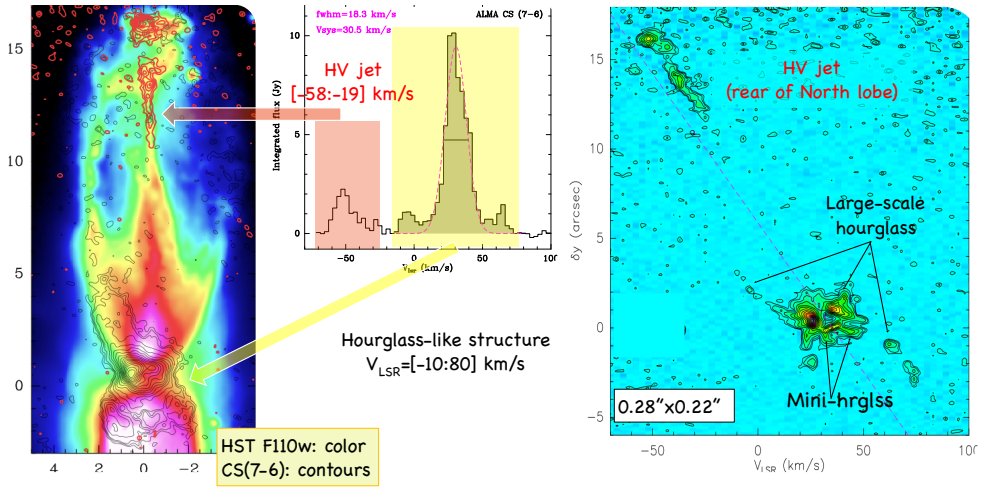


**Figure 4.** Overview of the CS (7−6) emission maps of OH 231.8+4.2 showing the integrated intensity map, atop the *HST*/F110W image (**left**), the one-dimensional spectral profile (**middle**), and the axial PV diagram (**right**). Different nebular components are indicated (namely, the large-hourglass, the HV-lobes, and the mini-hourglass). See text for details.

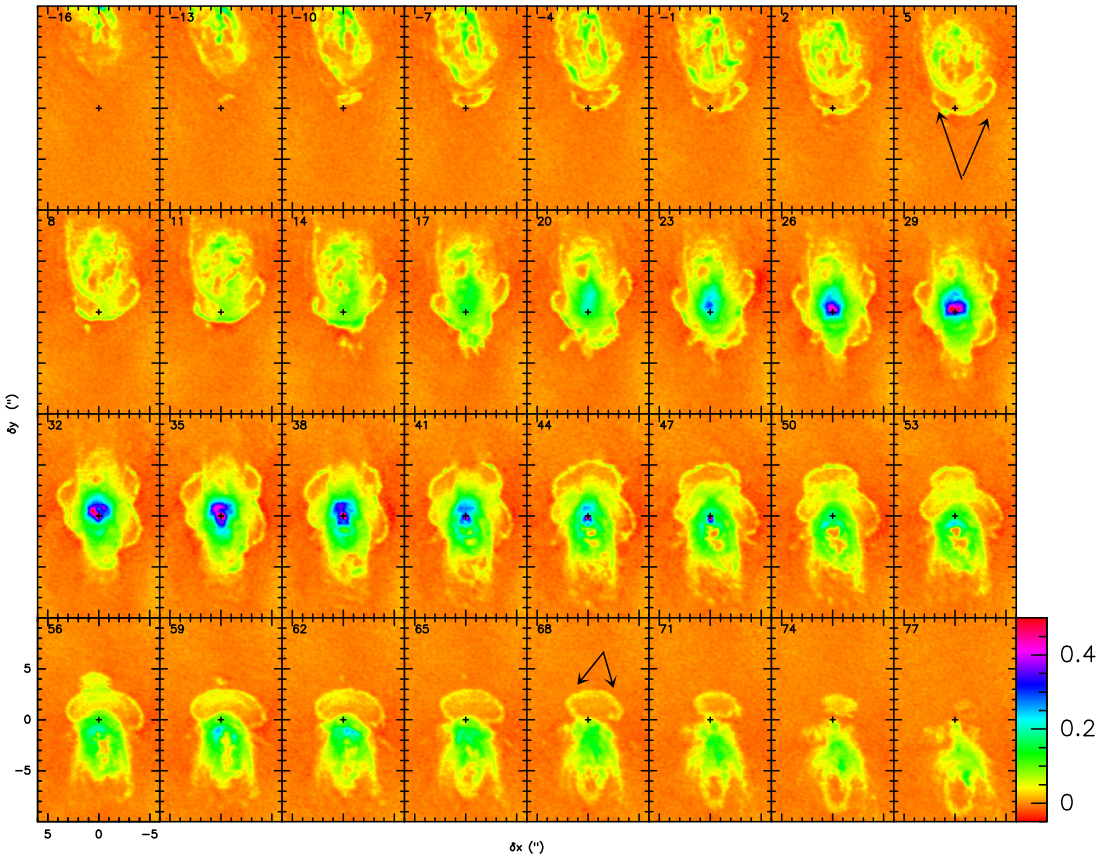


**Figure 5.** Velocity-channel maps of $^{12}$CO (3−2) in the velocity range where two faint, elongated bubble-like features (dubbed *the fish-bowls*) are discovered in the central regions of OH 231.8.

### *3.4. Conclusions*

Our ALMA observations of OH 231.8+4.2 unveil a series of new substructures that point to a nebular formation/shaping history significantly more complex than previously thought, and in particular, indicative of multiple non-spherical mass ejections. The origin of the bipolar ejections that

led to the formation of the outstanding nebular architecture of OH 231.8+4.2 remains unknown, but the presence of present-day bipolar ejections indicate that the CFW engine is still active at its core.

There are notable differences in the velocities and overall symmetry between the large-scale ∼800 yr old CO-outflow and the most current (≲80 yr old) bipolar ejections traced by SiO. These differences could indicate that the jet-launching mechanism itself has changed, or that the initial conditions under which the jets formed (presumably, involving disk-mediated mass transfer from the AGB to the companion star that blows the jets) have been modified in such a way that they now produce slower and more symmetric bipolar ejections than in the past. These changes may be intimately linked to major adjustments in the binary system configuration, which may have occurred after the powerful ejections that resulted in the formation of the massive and fast CO-outflow.

The position of QX Pup off-centre from the waist of the large-hourglass is one of the most puzzling discoveries from our ALMA data. Perhaps the combination of orbital motion and recoil of the binary system after strong asymmetrical mass ejections could explain, at least partially, its mysterious location. The orbital parameters of the central binary system are very poorly known. A loose upper limit to the orbital separation of $a < 150$ AU is deduced from the relative separation between clump *S* and the centroid of the SiO-outflow (presumably collimated by the companion).

New ∼0.″05-resolution observations with ALMA by our team (2017.1.00706.S) will enable us to determine the precise location of the SiO outflow engine relative to QX Pup and the scale at which the wind collimation begins, bringing us to the closest we have ever been to watching live the launch of a bipolar outflow from a mass-losing star and to understanding how OH 231.8+4.2 assembled its complex nebular architecture.

**Author Contributions:** C.S.C. has written this paper. All listed coauthors participated in the design of the observations, analysis and iterpretation of the data, and have contributed with comments to this manuscript.

**Funding:** Supported by the Spanish MINECO through grants AYA2012-32032, AYA2016-75066-C2-1-P, and AYA2016-78994-P and by the European Research Council through grant ERC-610256: NANOCOSMOS.

**Conflicts of Interest:** The authors declare no conflict of interest.

## References

1. Maercker, M.; Mohamed, S.; Vlemmings, W.H.; Ramstedt, S.; Groenewegen, M.A.; Humphreys, E.; Kerschbaum, F.; Lindqvist, M.; Olofsson, H.; Paladini, C.; et al. Unexpectedly large mass loss during the thermal pulse cycle of the red giant star R Sculptoris. *Nature* **2012**, *490*, 232–234. [CrossRef] [PubMed]
2. Balick, B.; Frank, A. Shapes and Shaping of Planetary Nebulae. *Annu. Rev. Astron. Astrophys.* **2002**, *40*, 439–486. [CrossRef]
3. Soker, N. Formation of Bipolar Lobes by Jets. *Astrophys. J.* **2002**, *568*, 726–732. [CrossRef]
4. Frank, A.; Blackman, E.G. Application of Magnetohydrodynamic Disk Wind Solutions to Planetary and Protoplanetary Nebulae. *Astrophys. J.* **2004**, *614*, 737–744. [CrossRef]
5. Van Winckel, H. Post-AGB Stars. *Annu. Rev. Astron. Astrophys.* **2003**, *41*, 391–427. [CrossRef]
6. Bujarrabal, V.; Alcolea, J.; Van Winckel, H.; Santander-García, M.; Castro-Carrizo, A. Extended rotating disks around post-AGB stars. *Astron. Astrophys.* **2013**, *557*, A104. [CrossRef]
7. Bujarrabal, V.; Neri, R.; Alcolea, J.; Kahane, C. Detection of an orbiting gas disk in the Red Rectangle. *Astron. Astrophys.* **2003**, *409*, 573–580. [CrossRef]
8. Bujarrabal, V.; Castro-Carrizo, A.; Alcolea, J.; Van Winckel, H.; Sánchez Contreras, C.; Santander-García, M.; Neri, R.; Lucas, R. ALMA observations of the Red Rectangle, a preliminary analysis. *Astron. Astrophys.* **2013**, *557*, L11. [CrossRef]
9. Bujarrabal, V.; Castro-Carrizo, A.; Alcolea, J.; Santander-García, M.; van Winckel, H.; Sánchez Contreras, C. Further ALMA observations and detailed modeling of the Red Rectangle. *Astron. Astrophys.* **2016**, *593*, A92. [CrossRef] [PubMed]
10. Bujarrabal, V.; Castro-Carrizo, A.; Alcolea, J.; Van Winckel, H.; Sánchez Contreras, C.; Santander-García, M. A second post-AGB nebula that contains gas in rotation and in expansion: ALMA maps of IW Carinae. *Astron. Astrophys.* **2017**, *597*, L5. [CrossRef]

11. Bujarrabal, V.; Castro-Carrizo, A.; Van Winckel, H.; Alcolea, J.; Sánchez Contreras, C.; Santander-García, M.; Hillen, M. High-resolution observations of IRAS 08544-4431. Detection of a disk orbiting a post-AGB star and of a slow disk wind. *Astron. Astrophys.* **2018**, *614*, A58. [CrossRef] [PubMed]
12. Bujarrabal, V.; Van Winckel, H.; Neri, R.; Alcolea, J.; Castro-Carrizo, A.; Deroo, P. The nebula around the post-AGB star 89 Herculis. *Astron. Astrophys.* **2007**, *468*, L45–L48. [CrossRef]
13. Bujarrabal, V.; Castro-Carrizo, A.; Alcolea, J.; Van Winckel, H. Detection of Keplerian dynamics in a disk around the post-AGB star AC Herculis. *Astron. Astrophys.* **2015**, *575*, L7. [CrossRef]
14. Kervella, P.; Homan, W.; Richards, A.M.S.; Decin, L.; McDonald, I.; Montargès, M.; Ohnaka, K. ALMA observations of the nearby AGB star L2 Puppis. I. Mass of the central star and detection of a candidate planet. *Astron. Astrophys.* **2016**, *596*, A92. [CrossRef]
15. Homan, W.; Richards, A.; Decin, L.; Kervella, P.; de Koter, A.; McDonald, I.; Ohnaka, K. ALMA observations of the nearby AGB star L2 Puppis. II. Gas disk properties derived from $^{12}$CO and $^{13}$CO $J = 3 - 2$ emission. *Astron. Astrophys.* **2017**, *601*, A5. [CrossRef]
16. Bujarrabal, V.; Castro-Carrizo, A.; Alcolea, J.; Sánchez Contreras, C. Mass, linear momentum and kinetic energy of bipolar flows in protoplanetary nebulae. *Astron. Astrophys.* **2001**, *377*, 868–897. [CrossRef]
17. Alcolea, J.; Bujarrabal, V.; Sánchez Contreras, C.; Neri, R.; Zweigle, J. The highly collimated bipolar outflow of OH 231.8+4.2. *Astron. Astrophys.* **2001**, *373*, 932–949. [CrossRef]
18. Bujarrabal, V.; Alcolea, J.; Sánchez Contreras, C.; Sahai, R. HST observations of the protoplanetary nebula OH 231.8+4.2: The structure of the jets and shocks. *Astron. Astrophys.* **2002**, *389*, 271–285. [CrossRef]
19. Sánchez Contreras, C.; Bujarrabal, V.; Miranda, L.F.; Fernández-Figueroa, M.J. Optical long-slit spectroscopy and imaging of OH 231.8+4.2. *Astron. Astrophys.* **2000**, *355*, 1103–1114.
20. Sánchez Contreras, C.; Desmurs, J.F.; Bujarrabal, V.; Alcolea, J.; Colomer, F. Submilliarcsecond-resolution mapping of the 43 GHz SiO maser emission in the bipolar post-AGB nebula OH231.8+4.2. *Astron. Astrophys.* **2002**, *385*, L1–L4. [CrossRef]
21. Sánchez Contreras, C.; Gil de Paz, A.; Sahai, R. The Companion to the Central Mira Star of the Protoplanetary Nebula OH 231.8+4.2. *Astrophys. J.* **2004**, *616*, 519–524. [CrossRef]
22. Matsuura, M.; Chesneau, O.; Zijlstra, A.A.; Jaffe, W.; Waters, L.B.F.M.; Yates, J.A.; Lagadec, E.; Gledhill, T.; Etoka, S.; Richards, A.M.S. The Compact Circumstellar Material around OH 231.8+4.2. *Astrophys. J.* **2006**, *646*, L123–L126. [CrossRef]
23. Forde, K.P.; Gledhill, T.M. Discovery of shocked H2 around OH 231.8+4.2. *Mon. Not. R. Astron. Soc.* **2012**, *421*, L49–L53. [CrossRef]
24. Balick, B.; Frank, A.; Liu, B.; Huarte-Espinosa, M. Models of the Hydrodynamic Histories of Post-AGB Stars. I. Multiflow Shaping of OH 231.8+04.2. *Astrophys. J.* **2017**, *843*, 108. [CrossRef]
25. Sánchez Contreras, C.; Alcolea, J.; Bujarrabal, V.; Castro-Carrizo, A.; Velilla Prieto, L.; Santander García, M.; Quintana-Lacaci, G.; Cernicharo, J. Through the magnifying glass: ALMA acute viewing of the intricate nebular architecture of OH231.8+4.2. *Astron. Astrophys.* **2018**, forthcoming. [CrossRef]